の予測が立つためのイメージング，また，今ある心筋が本当にだめなのかどうかということがみられるイメージング，そのようなイメージングがほしいですね。

心不全・不整脈疾患

内藤　そういう意味合いで，虚血性心疾患と動脈硬化症の次の心臓病治療のターゲットとなるのがたぶん，心不全と不整脈だと思います。心不全の画像診断は心機能の診断法としてないわけではないのですが，不整脈の画像診断となると，今まであまり一般的ではありません。この領域に関する画像診断の将来展望はいかがでしょうか。

田中　テーマが心不全ということでかなり漠然としているのですが，心不全を起こす疾患は，虚血，心筋症，弁膜症が大きなカテゴリーだと思うのです。それらを総合的に評価し，みていくことが必要だと思います。今心筋と冠動脈に関してはかなりイメージングが発達しているのですが，弁をどうみていくかというと，現時点では超音波しかありません。その超音波の評価はかなり operator dependent の部分があり，客観的に手術にもち込むまでのイメージングとして活用できている状態ではありませんでした。しかし，現状では，MRI や CT の時間分解能や空間分解能がかなりよくなり，みることができる可能性が出てきたと思いますので，今後数年は弁のイメージングも重要になってくるのではないかと考えています。

それと同時に，弁の機能不全を来たす疾患の1つに虚血があります。心室基部の虚血によって弁輪が拡張して弁逆流が起こってくる病態ですね。その時にどの程度心筋がダメージを受け，それが不可逆的なダメージになりリモデリングするのか。そのままで自然治癒してリモデリングし，逆流を抑えることができるようになるのかを判定する方法として，イメージングの位置付けが1つあってもいいのではないかと思います。

内藤　多田村先生，心機能の評価法についていかがですか。

多田村　現在，MRI が評価法のゴールドスタンダードです。それが，そのまま将来に向けてもっと使われるようになるのではないでしょうか。ただ，たとえばペースメーカーが埋め込まれている患者さんや，どうしても MRI ができない閉所恐怖症のような人を客観的に評価したいのであれば，CT なら心機能評価だけであれば造影剤量を減らしてもできますし，冠動脈の 1/4 くらいの線量でも可能ですので，そういった人のフォローに使われていく可能性があるのではないかと思っています。

内藤　心機能の診断方法は昔から数多くあるのですが，何をどこまで，どの程度の精度で評価すれば許されるのかということ自体ずっとゴールがないという状況ですね。たとえば，左室機能の指標としては超音波による簡単な fractional shortening だけでも患者さんのマネージメントはそれなりにできますが，一方で，もっと厳密な指標がほしいという方向もあります。私個人の感覚からいうと，ejection fraction よりも何かもう少し心機能をみるいい指標を求めなければならないのではないかと思います。角辻先生，心機能の評価法というのはいかがですか。

角辻　イメージングをどのタイミングで何に使うか，ですね。心不全の経時的フォローアップには今使われている心エコーでの経時的な観察によって各ポイントの心臓の状態がある程度わかり，臨床的には十分使えていると思います。ただ，田中先生が言われたように，エコーの問題の1つに operator dependent という問題があり，「この人はこういうけれども，あの人はこういう」というあやふやさが残っているのは時に大きな問題となります。たとえば心筋にしても，ここは本当にダメ

ージで，もう修復できないのか，それとも，可能性が残っているかどうかということは，突き詰めていくと本当はわかりません。 これから10年の間に治療に直結してくる情報をきっちり出してくれるイメージングが絶対にほしいと思います。

内藤 局所の心筋の状態を画像できっちりみられる方法はありますか。

角辻 MRIは全体的にきれいにみえます。エコーでもある程度わかりますけれども，検査をする人によって結果が違う可能性があるというのが今の現実だと思います。冠動脈を把握することがより簡便になり，心臓全体として，だれもが同じ意思決定ができるほどの確たる情報を出してくれる手軽なイメージングがほしいですね。

内藤 血液指標としてはBNPなどで判断されていることも多いかと思うのですが，このへんの心筋が弱っているということが画像できっちりわかると，さらによいということですね。

角辻 インターベンションや手術など，何か大きな治療をするかどうかを決定する際には，BNPだけではどこの時点で何をするのかを決定するには足りないと思います。

内藤 わかりました。

専門領域における将来の夢

内藤 最後に，画像診断を絡めた，ご出席の先生方の専門領域における将来の夢を語っていただいて終わりにしたいと思います。

角辻 第1は心筋梗塞を予防できるイメージングがほしいと思います。特に心筋梗塞により重症になってしまう患者さんを何とかしたい。元来重症冠動脈疾患をもっている患者さんの心筋梗塞では，心臓は救えても脳に異常が出てしまうなど，ものすごく残念なことになる患者さんが多いわけです。それを救うために，スクリーニング的なプラークのイメージング評価がほしいです。

第2は，私はinterventionalistなのでイメージングをインターベンションにうまく活用することを考えています。きっちりとした結果を患者さんに与えなければいけないにもかかわらず，施設によってインターベンションにおいて差があるのが現状だと思います。統一された結果を出せるインターベンションをしっかり行うためのイメージングがほしいですね。私は血管造影だけでは不足であると思います。血管造影とともにIVUSや内視鏡などが複合的に使えるようになるべきです。今，3Dかつ GPSで誘導するようなシステムも作られているのですが，それほどの機能ではなくとも，それに近い情報を血管造影に複合的に入れていけるイメージングが絶対に必要になってくるし，できてくると思っています。

内藤 多田村先生，いかがですか。

多田村 先ほど角辻先生が言われたviabilityの問題においても，AHAのガイドラインのPCIの適用基準もあいまいで，それを信じない人もいます。私もそれが絶対ではないことはわかります。循環器医療はある意味リスクが高いか低いかという確率論の領域となり，確固たるものはなかなか出ません。「ここからここは絶対にだめで，ここからここはOK」というものではないと思っています。将来イメージングが鮮明になったからといって動脈硬化や心筋梗塞の発症率や，弁膜症の手術適応などの確固たるものが出る類の領域ではないのではないでしょうか。ただ，いろんな組み合わせでもいいのですが，治療法の適用を決めるイメージングの使用法は重要かつ必要です。そういうエビデンスを出すためにはすごく大規模な治験をせざるを得ないと思うのですが，今後もそのようなことをせず，医師の勘に頼った医療がずっと続いていくのではないかという懸念もあります。

内藤 循環器病というのは，癌のようにもともと身体の中になかったものが急速に出てくるわけ

ではなく，ある程度連続的な変化の中で捉えられるものです。そういう意味合いからいえば，もちろん予防という考えも通用するでしょうし，癌のように早期発見，早期治療というよりも，適切な時期に適切な治療を行うことがさらに重要といえます。そういう疾患の違いは当然あると思います。ですから，どのように予防するのか，あるいは，どの時期に，どういう治療を行うのかということはエビデンスに基づかなければいけないでしょうね。ただ，EBM（evidence-based medicine）という言葉自体は，エビデンスを集めて盲目的にそれに従うだけではなく，エビデンスをもとにその患者さんにとって，あるいはその施設で一番よい方法を選ぶというのが本来の意味だと思うので，それをさらに進めていくことだと考えてよろしいでしょうか。

多田村　そのエビデンスが患者さん個々に当てはまるかどうかというのはまた別の問題なので，もちろん個々に裁量があって当然だと思います。

内藤　田中先生はいかがですか。

田中　今までの流れと全く話が違いますが，今までの循環器イメージングというのは，血管造影から移行してきた部分が多いと思うのです。超音波というmodalityは以前からある程度確立した役割を果たしてきましたけれど，現在のCTやMRIというmodalityに関しては，いかに血管造影を置き換えていくのかという時代から始まり，ある程度置き換わりつつある時代に来たと思っています。ですから，将来的にはそれをさらにbrush-upし，精度の高い機械に完全に置き換えることができる可能性はあると思います。

また，機械はどんどん発達し，さまざまな施設にも導入されているにもかかわらず，それをうまく使いこなしていない現実があります。それをソフト面でどのように解決していくのかということが大きな問題だと思います。それは画像診断，イメージングとしてのソフト面も当然そうですし，それに追従するものとして治療のソフト面も変わってくるべきだと思います。それを今後5年，10年で広げていくことが1つの夢というか，方向性なのかなと考えています。

そのためには，今の技術をより成熟させ，簡便にだれでも使えるわかりやすい機械にし，フィードバックしていくことも必要でしょう。また，それに新たな技術をつけ加えて最先端な治療を行っていかなければなりません。近い将来，特にCTでは256列という多列化のmodalitiyも出てきますし，時間分解能を上げていくdual source imagingという新しい概念も出てきていますので，そういうものをどう組み合わせて疾患に応用していくかということが重要ですね。10年先はわかりませんが，5年ぐらい先は大きく変わると思いますので，それに対して何かいい回答が出せればいいなと考えています。

内藤　皆様方の先ほどからの議論に出てくる1つのポイントは「客観化」ではないかと思います。画像診断にしろ，治療にしろ，ある程度高いレベルの診断や治療が客観的にだれにでもできるという時代が1つの理想かと思います。しかしそうなると，われわれは何をすればいいのかと。逆に職がなくなってしまうかもしれないという懸念を表して，これで終わりにしたいと思います。

皆さん，どうもありがとうございました。

（了）

大動脈疾患

画像所見

70歳代，男性．既往歴に肺結核，高血圧があった．食事をすると飲み込みにくく腹部膨満があるため近医を受診．胸腹部CTにて胸腹部大動脈瘤を指摘された．入院時脈拍は74/分・整で，血圧は130/70mmHg（左右差なし）であった．大動脈瘤は3D-CTにて嚢状（図1，2；→）で，横断面での最大短径は46mmであるが，単軸断面で計測したサイズは大動脈を含め67mm程度と判明した．一部，瘤内壁在血栓側に凸な血流腔を認める（図1；→）も，瘤そのものはほとんどが血栓により占められていた．CT検査の翌日の夜に腹痛が出現し眠れないとの訴えがあったため，その3分後に訪室するとうめき声をあげ顔面蒼白となっており，呼びかけに反応しなくなりCPAとなった．直ちに蘇生術を行うも血圧触知せず，心拍数30～40．エコー上右胸水著明のため胸腔ドレナージ施行，血液1500ml流出あり，胸腹部大動脈瘤破裂によるショックと考えられた．蘇生を続けたが反応なく，死亡を確認した．

病理所見

大動脈の内腔からの肉眼所見では内膜の一部が欠損して瘤腔に連続しており，仮性動脈瘤であった．また，胸腔側からの観察では破裂点は瘤の頂点より下部の遠位側であった（図3；→）．瘤内には血栓が見られたが，内膜欠損部と破裂点とは必ずしも近い部位ではなく，血栓内の脆弱な部分を分け入るように血流腔が伸展して瘤壁に到達し，瘤壁が最も脆弱な部位で破裂したと考えられる（図4；→）．

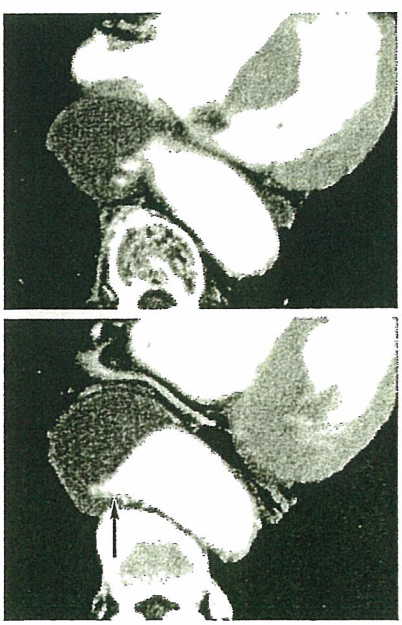

図1　造影CT像（破裂前日）

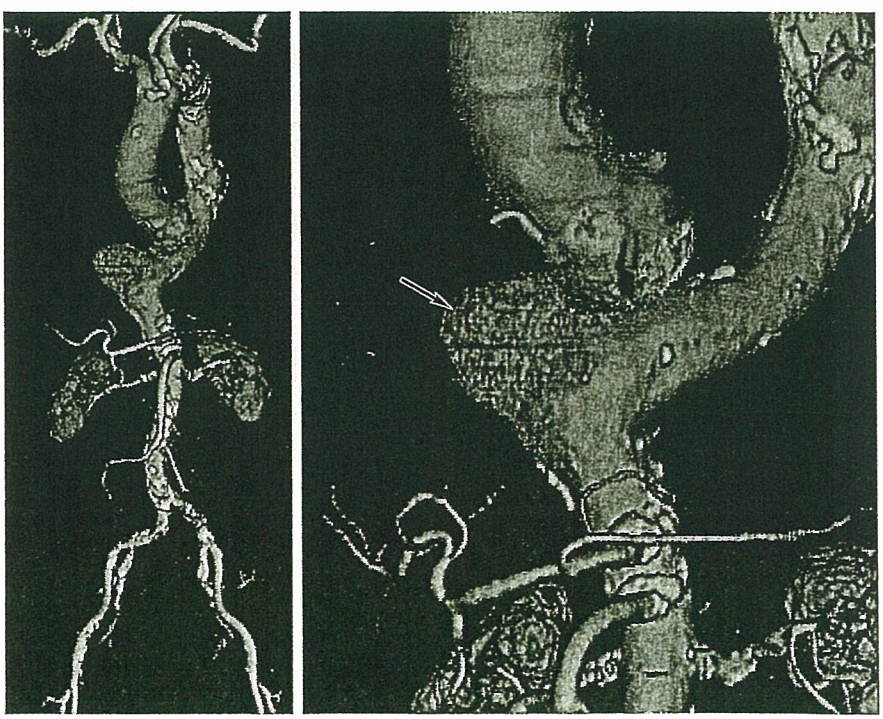

図2　3D-CTAボリュームレンダリング像

画像と病理像との対比

本例では瘤壁は外膜および一部内膜を持つ構造であり，内膜を伴わない仮性瘤の状態で，penetrating atherosclerotic ulcer[1] から瘤化し，壁内血腫を形成した状態であったと考えられる．しかし，破裂の前日に施行されたCTでは内膜を同定することは困難で，仮性瘤と真性瘤を鑑別することは難しい．一方で血腫内に入り込んだ血流腔は，retrospectiveに検討すると，内膜欠損部から瘤内に伸展した血流腔とよく一致していることがわかる．また，嚢状の瘤の形態は，当然ながら剖検で確認された瘤の形態と一致しており，伸展した血管壁（外膜）に覆われた瘤であることは容易に想像できる．CTでは内膜そのものを描出することは困難であるため，厳密に真性瘤であるか仮性瘤であるかを鑑別しえないが，嚢状瘤で，内腔面に不整な血流腔がある場合は，このような病態を念頭に置き診療にあたることが重要と考えられる．

■文献

1) Stanson AW, Kazmier FJ, Hollier LH, et al: Penetrating atherosclerotic ulcers of the thoracic aorta: natural history and clinicopathologic correlations. Ann Vasc Surg 1: 15-23, 1986.

国立循環器病センター放射線診療部
現）岩手医科大学放射線科
田中良一

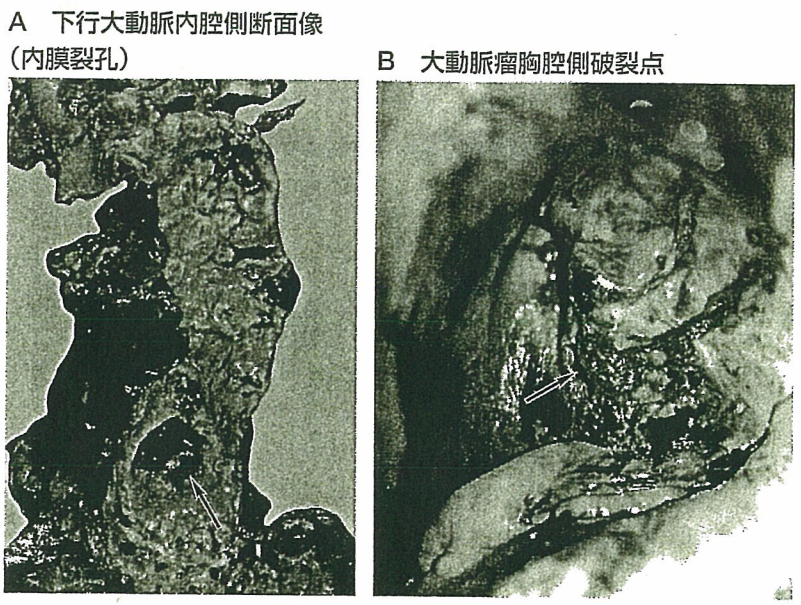

図3

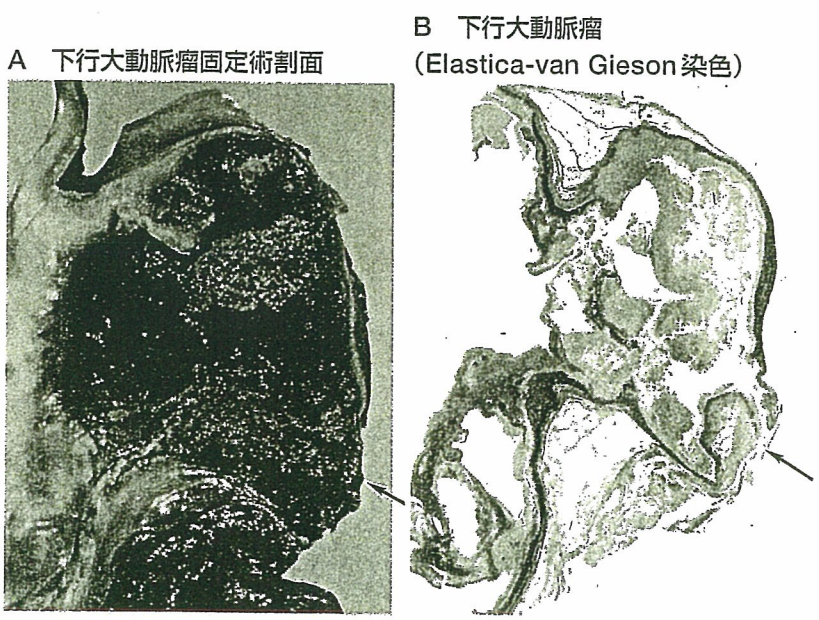

図4

CHAPTER 64

Nanofabrication of Inorganic-Organic Composites by Chemical Bonding for Medical Devices

Tsutomu Furuzono, Shoji Yasuda, Masahiro Okada

Department of Bioengineering, National Cardiovascular Center Research Institute, Osaka, Japan

CONTENTS

1. INTRODUCTION

Hydroxyapatite [HAp: $Ca_{10}(PO_4)_6(OH)_2$] has unique properties for biomaterials such as hard-tissue-compatible material for bone and tooth also soft-tissue-compatible material for skin tissue [1]. The reasons for the compatibility have not been manifested completely. One of them might be favorable to adsorption of adhesion molecules or growth factors *in vivo* on the HAp surface [2]. The HAp as biomaterials is prepared artificially through the following processes: wet method using solution reaction from solution to solid, dry method using solid reaction from solid to solid, hydrothermal method using hydrothermal reaction from solution to solid, and alkixide method using solution and solid reaction from solution to solid [1]. The HAp can be obtained as some morphologies such as powder-, needle-, rod-, fiber-, porous-like, and so on. From the point of view of tissue-compatible material made up of HAp, the hard and brittle nature of HAp limits spreading over many medical applications.

Recently, many synthetic methods for the HAp composites to overcome such defects of HAp have been reported.

ISBN: 1-58883-079-9

Bottom-Up Nanofabrication
Edited by Katsuhiko Ariga and Hari Singh Nalwa
Pages: 1–18

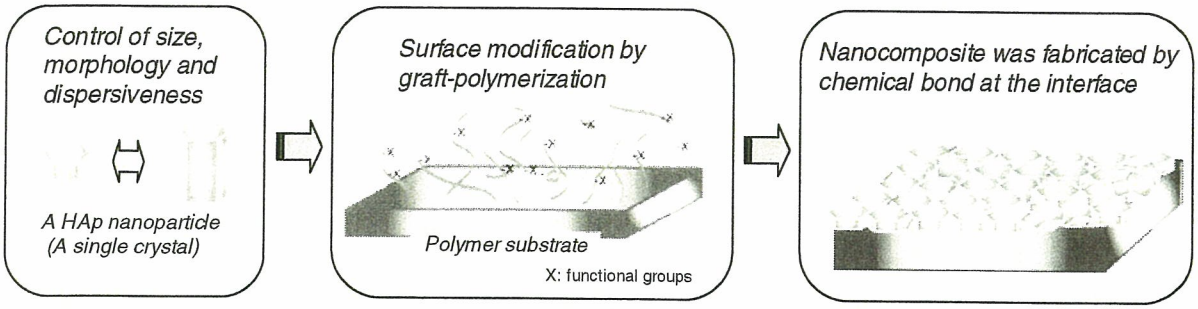

Scheme 1. Schematic presentation of an inorganic-organic composite material by chemical bonding between the interface.

These methods of development of inorganic-organic composites are effective to give elasticity or flexibility to the inorganic material. For example, there were the effective methods which dispersed HAp crystals into polymer matrix [3–6], preparation of a self-organized composite consisting of HAp and collagen molecule using a coprecipitation method [7–9], formation of HAp crystals on polymer substrate by a biomimetic process using a simulated body fluid [10, 11], rapid formation of amorphous HAp on polymer substrate by an alternate soaking process [12–14], and preparation of composite using a plasma spraying [15].

To overcome the defects of ceramics maintaining the nature of HAp, we developed a novel inorganic-organic composite, which calcined HAp nanoparticles (crystals) [16, 17] coated on polymer substrate by chemical bonding, such as covalent or ionic linkage [18–22]. The synthetic method of the nanocomposite was quite different from the others, which were prepared by mixture with HAp crystals and polymer matrix or formation of amorphous HAp on polymer surface. The significant feature of our fabrication is formation of a nanoscaled ceramic layer on substrate surface without damage to the mechanical properties of the polymer substrate. The technology of nanoceramic coating can be applied to the increase of adhesiveness between hard materials and soft tissue in a living body, and developing novel biomaterials compatible for soft-tissue, such as percutaneous device, artificial blood vessel, or a scaffold for regenerative medicine.

The design of the nanocomposite, consisting of calcined HAp nanoparticles and polymer substrates, depends on two key technologies: (1) control of size, morphology, and dispersiveness of calcined HAp nanoparticles and (2) fabrication of inorganic-organic composite by chemical bonding between the interface as shown in Scheme 1.

In this chapter, we present the synthetic method of the calcined HAp nanoparticles with controlled size, morphology, and dispersiveness in a liquid media, and synthesis of the nanocomposite, and also the surface, mechanical, and biological properties of the material as well as fabrication of medical devices in detail.

2. CALCINED HAp NANOPARTICLES FOR NANOFABRICATION

2.1. Background

Previously, Aoki et al. demonstrated that sintered Hap—a ceramic disk—-showed excellent biocompatibility with soft tissues of the skin, muscle, and gums and designed a percutaneous catheter with HAp disk to prevent infection [23]. However, the device as a rigid ceramic disk that partially protrudes through the skin might limit patient mobility and caused discomfort. To overcome the disadvantage, Zabetakis et al. prepared a flexible polymeric catheter with thin film of HAp laid down by pulsed laser deposition method [24]. However, there were many cracks in the HAp coating on the polymer substrate because there was weak interaction between coated HAp and the surface of catheter. The preliminary implant test using this material also showed minimal inflammatory response in subcutaneous tissue of rat due to the amorphous HAp coating.

We demonstrated a novel sintered HAp microparticles coating onto silicone substrate with covalent linkage [25, 26]. We can expect to not only develop a new technique for HAp nucleation on an inert polymer surface but also prepare a more stable composite consisting of HAp layer and polymer substrate bonded with covalent linkage. The adhesion strength between particle and polymer substrate, however, was believed to be unsatisfactory because a commercial grade of HAp spherical particle with 2.0 μm of an average diameter was used in this system. To increase the interaction between a HAp particle and substrate surface, we need to synthesize a HAp nanoparticle with larger surface area of adhesion to avoid strong shearing stress from outside. Here we described the characterization of calcined HAp nanoparticles synthesized by a modified emulsion system above and below the temperature of a surfactant's cloud point [16, 17]. The HAp nanoparticle can be a well-controlled size and morphology and also showed dispersiveness in a liquid media.

2.2. Control of Size and Morphology

Some synthetic methods of HAp nanoparticles have been previously reported, such as wet chemical process [27–29], hydrothermal treatment [30–32], sol-gel process [33–35], and emulsion system [36–38]. Calcined HAp nanoparticles were prepared by a modified emulsion system. Starting materials were dodecane [$CH_3(CH_2)_{10}CH_3$], as a continuous oil phase, pentaethylene glycol dedecyl ether [$CH_3(CH_2)_{10}CH_2O(CH_2CH_2O)_4CH_2CH_2OH$], as a nonionic surfactant showing 31°C of the cloud point by our experimental measurement, calcium hydroxide [$Ca(OH)_2$] and potassium dihydrogen phosphate (KH_2PO_4). The 10 ml of 2.5 M $Ca(OH)_2$ aqueous suspension was poured into 40 ml

of the oil phase containing of 0.5 g of the surfactant at 25° and 50°C. After rapidly stirring of the water/oil (W/O) solution, 10 ml of 1.5 M KH_2PO_4 aqueous supersaturated solution was added into the W/O system. After stirring for 24 h at the fixed temperature, the inorganic reactant was obtained by centrifugation with ethanol and hot water to remove the oil and the surfactant. The powder was dried at 60°C for 12 h and then calcined at 800°C for 1 h with a 10°C/min of the heating ratio.

Figure 1 indicates X-ray diffraction (XRD) patterns of the both calcined HAp powders at 800°C. In all the figures in this section, the (a) represents HAp particles prepared by the emulsion system at 25 and (b) represents 50°C. Both profiles showed the presence of highly crystalline HAp, no other calcium phosphate phases could be detected. Lim et al. reported that high-purity crystalline HAp powder prepared at the same calcination temperature was obtained through an emulsion processing rout, however in conventional process impurity phase of β-$Ca_3(PO_4)_2$ was obtained [39]. Similarly, since there was no impurity crystalline except for HAp in our XRD result, our method lead to the formation of a more homogeneous precursor than that formed in the conventional route.

Figure 2 shows the FT-IR spectra of the calcined HAp powders synthesized at (a) 25°C and (b) 50°C. In the spectra, bands at 603/573 and 474 cm^{-1} represent ν_4 PO_4^{3-} and ν_2 PO_4^{3-} in Hap crystalline, respectively. Peaks at 964 cm^{-1} reflected ν_1 PO_4^{3-} and 1091/1052 cm^{-1} for ν_3 PO_4^{3-}. The strong intensities of the OH stretching and libration at 3572 and 632 cm^{-1}, respectively, indicate a well-crystallized product. The bands at 871 and 1420–1470 cm^{-1} showed B-type carbonate apatite which carbonate substituted phosphate positions in the lattice of HAp [40]. Since carbonate apatite is known to be a better biomaterial than pure HAp [$Ca_{10}(PO_4)_6(OH)_2$] due to the similarity to the composition of biological apatite [41], the HAp particles obtained in this study are expected to show bioactivity. The Ca/P molar ratios in the particles prepared in both systems was 1.61 as

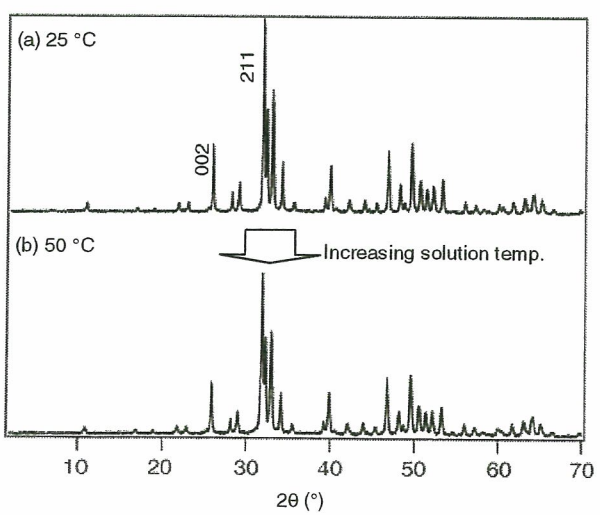

Figure 1. XRD profiles of the calcined HAp nanoparticles synthesized at (a) 25°C and (b) 50°C.

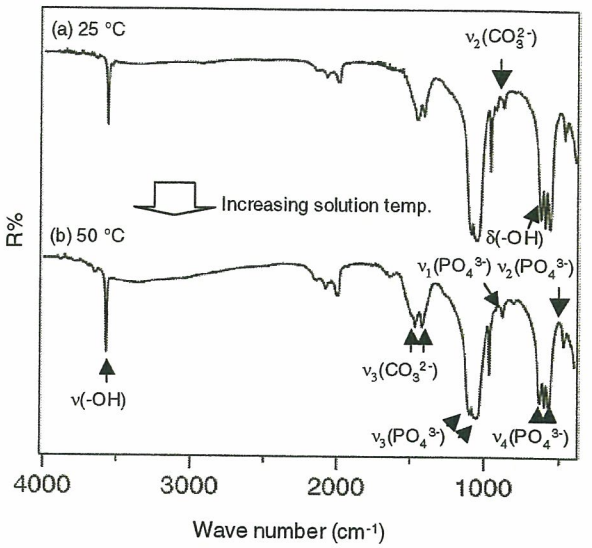

Figure 2. FT-IR spectra of the calcined HAp nanoparticles synthesized at (a) 25°C and (b) 50°C.

determined by ICP, slightly less than a stoichiometric composition 1.67. This value implied that this powder was slightly calcium defect.

Figure 3 shows the particle morphologies by transmission electron microscopy (TEM) observation. The HAp particles prepared at 25°C and then calcined at 800°C were

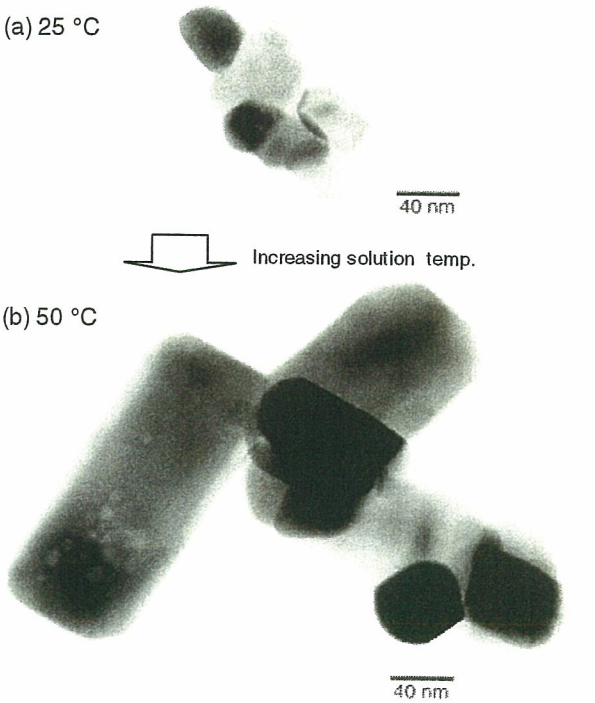

Figure 3. TEM micrographs of the calcined HAp nanoparticles synthesized at (a) 25°C and (b) 50°C.

agglomerates of particles, which showed a spherical to irregular rod shape with the particle size of 30–60 nm (Fig. 3(a)). However, the HAp particles prepared at 50°C were truncated rod shaped with distinct beveled corners at the apex. These particles were generally larger sized, 100–200 nm in length and 90–150 nm in width (Fig. 3(b)). The electron diffraction pattern that correspond to HAp crystalline structure was obtained (inset in Fig. 4). As shown in Figure 4(b), the longitudinal axis of the rod-shaped crystal was parallel to the *c*-axis of the HAp lattice.

The difference in the morphology and size of the both particles prepared in this study is believed to be a consequence of the different temperatures employed. The morphology and size of an HAp particle previously made by an emulsion route shows a spherical to irregular rod shape with the size of 20–100 nm [42, 43]. At 25°C in our system, an immediate onset of white cloudiness with the addition of phosphate solution without precipitation indicates that precipitation occurs within the many dispersed nucleation centers formed by the surfactant-bounded micelles. It is likely that initially the micelles interact and exchange contents. Calcium phosphate nucleation occurs within the micelle cavity and micelles then merge to some extent at early stage crystal growth and the crystal enlarges. A stable emulsion is thus maintained and roughly spherical crystals are finally formed, confined within an adsorbed surfactant boundary.

When the reaction temperature increases to 50°C beyond the cloud point, it is assumed that the shaped vesicle might be no longer able to maintain its thermodynamic stability in the emulsion system due to the increase of hydrophobicity of the surfactant molecule. After addition of the aqueous $Ca(OH)_2$ suspension, calcium ion might bind to the locally and partially remained hydrated oxyethylene branch containing a hydroxyl head group in the surfactant molecule, resulting in the formation of local hydration space. Subsequently, such hydration space could nucleate calcium phosphate upon addition of the KH_2PO_4 solution. The HAp crystal growth is then significantly faster than that at 25°C as the driving force of the crystal growth remarkably plausibly preceded the formation force of the locally assembled hydration space because of the enhanced hydrophobicity of the surfactant. The morphological development of the crystal is only moderately modified from the needle-like crystals that develop from a surfactant free system. Low aspect ratio HAp crystals develop, indicating there is some interaction of surfactant with the crystal faces, particularly the fastest-growing (001) face, as indicated by the unusual truncation of this face. This scheme resembles an effect of face-specific additive that inhibits the crystal growth results in an increase in the relative area of that face as growth proceeds [44].

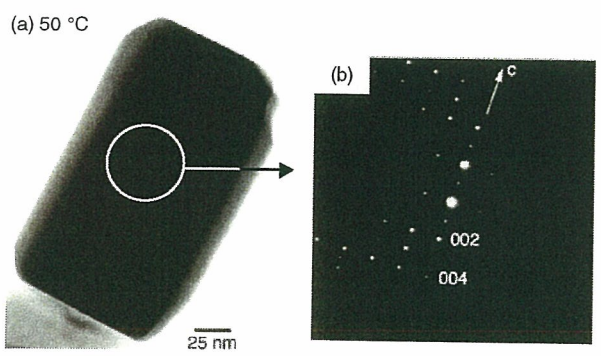

Figure 4. TEM micrographs of prepared HAp nanoparticles obtained after calcining; (a) prepared at 50°C showing truncated faces and elongation along *c*-axis; (b) associated ED pattern corresponding to [0 1 0] zone.

2.3. High Dispersibility

When low-crystallinity HAp nanoparticles are calcined to increase thermal and chemical stability, the particles typically sinter into large agglomerates [45–49]. Consequently, calcined HAp crystals dispersed in liquid medium on a nanoscale have been difficult to obtain. Hydrothermal treatment of HAp particles in water medium under high pressure is known to enable the preparation of agglomerate-free HAp crystals [29–31]. However, this treatment generally leads to an increase in crystal size due to Ostwald ripening [50, 51] and is restricted to laboratory-scale products as it is a high-pressure process.

This subsection describes the preparation of HAp nanoparticles by calcination with an antisintering agent interspersed between the particles and the subsequent removal of the agent. There was no contact between the particles during calcination. $Ca(OH)_2$ was selected as an antisintering agent because it would not melt at the calcination temperature (800°C), presumably not dissolve the HAp, and could be removed by washing with water after calcination. The HAp nanoparticles obtained here should be suitable for the surface coating described the later section owing to their high dispersibility in liquid media and high thermal and chemical stability.

2.4. Synthesis and Characterization

Starting HAp particles with low crystallinity were prepared by a modified emulsion system at 25°C [16, 17]. The resulting product was centrifugally washed and redispersed in water (solid content: 5 wt%). To intersperse $Ca(OH)_2$—an antisintering agent—between the particles, the HAp aqueous dispersion was added into a saturated aqueous $Ca(OH)_2$ solution (0.17 wt%), and the mixture was dried under reduced pressure at 40°C. The resultant HAp/$Ca(OH)_2$ (1/1, w/w) mixture was calcined at 800°C for 1 h in air (heating rate: 10°C/min). After calcination, the mixture was centrifugally washed with water to remove the $Ca(OH)_2$. As a control, HAp was calcined using the same procedure, but without adding $Ca(OH)_2$.

X-ray diffraction measurement was carried out for the caldined HAp particles at 800°C for 1 h with $Ca(OH)_2$ interposed among the crystals. After calcination, $Ca(OH)_2$ was removed by centrifugal washing with water. The XRD profiles showed highly crystallized HAp, and no other calcium phosphate phases could be detected. This result indicates that the heat treatment with $Ca(OH)_2$ at 800°C for 1 h did not influence the crystal phase of HAp. The sizes of the crystals dispersed in ethanol measured by dynamic light scattering were quite different between the two kinds of the calcined HAp with and without $Ca(OH)_2$ as shown in Figure 5.

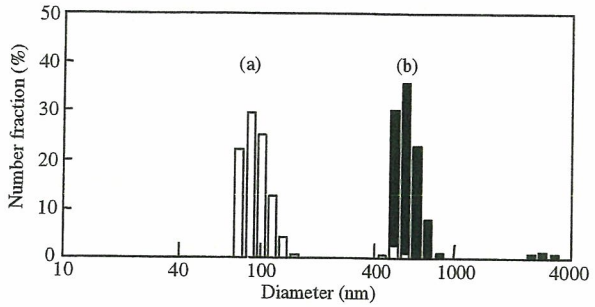

Figure 5. Size distributions of HAp particles calcined at 800°C for 1 h with (a) and without (b) an antisintering agent, PAA-Ca, surrounding the HAp particles followed by washing with water to remove the thermal decomposed product of PAA-Ca, CaO. The size distribution was measured in ethanol as a medium by using dynamic light scattering.

In the case of calcination without $Ca(OH)_2$, shown as the solid columns, the mean size of the HAp crystals dispersed in HAp crystals were dispersed as agglomerates consisting of sintered polycrystals whose mean size indicated about 600 nm. However, calcining with the antisintering agent, the mean size of the crystals was much smaller than that without the agent. The average size of the HAp nanoparticles was about 80 nm. The results indicate that the sintering among HAp nanocrystals could be avoided by calcination with $Ca(OH)_2$ interposed among the crystals, followed by the removing of $Ca(OH)_2$ after calcination. From electron microscope observations, the size of the HAp crystals was ranged from 50 to 100 nm, which was irrespective of the calcination with or without $Ca(OH)_2$, as shown in Figure 6 as well as Figure 5(a). The HAp nanoparticles were scattered by a single particle on a scanning electron microscopy (SEM) mount. The higher magnification TEM image of a particle calcined with $Ca(OH)_2$ and its electron diffraction pattern (Fig. 6(b), 6(c)) confirmed that the particle was a single HAp crystal with an irregular spherical morphology.

Calcined HAp nanocrystals with a rodlike morphology were also obtained with poly(acrylic acid–Ca salt) (PAA-Ca) as the antisintering agent surrounding the particles followed by removal of the agent. The SEM and TEM/ED images were shown in Figure 7. The HAp nanoparticle, which showed also a single crystal (Fig. 7(c)), definitely

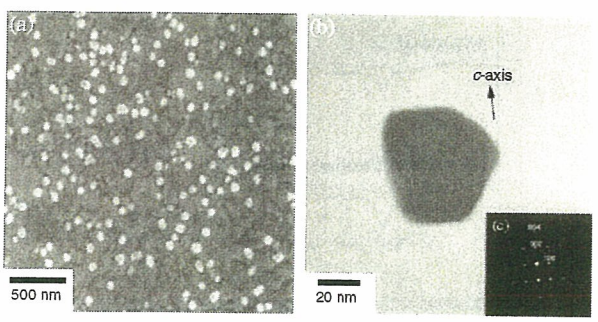

Figure 6. SEM photograph (a), TEM photograph (b), and the associated electron diffraction pattern (c) of spherical HAp crystals calcined at 800°C for 1 h with an antisintering agent, PAA-Ca, followed by washing with water.

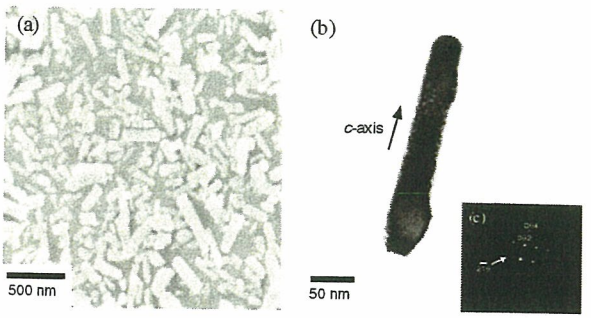

Figure 7. SEM photograph (a), a TEM photograph (b), and the associated electron diffraction pattern (c) of rodlike HAp crystals calcined at 800°C for 1 h with an antisintering agent, PAA-Ca, followed by washing with water.

elongated to *c*-axis and was scattered by almost a single one in SEM image (Fig. 7(a)).

The HAp nanocrystals calcined with PAA-Ca showed high dispersibility in liquid media and a large specific surface area due to the antisintering effect of PAA-Ca surrounding the particles. Also, the HAp crystals calcined with PAA-Ca showed highly crystallinity, and no other calcium phosphate phases could be detected. The HAp nanocrystals obtained here should be suitable for various applications, such as biomaterials, ion exchangers, adsorbents, catalysts, and dental and orthopedic ultrafine fillers for microporosity owing to their high dispersibility in liquid media and high thermal and chemical stability. Calcination with an antisintering agent has potential application to a wide range of calcined nanoceramic powders, such as alumina, titania, and magnesia, and offer significant benefits over existing technologies because the technique is simple, inexpensive, and amenable to scaling up and processing.

3. HAp NANOCOATING BY CHEMICAL BONDING

3.1. Background

The surface of HAp crystal possesses hydroxyl groups and calcium and phosphate ionic sites to react with chemical functional groups of organic molecules. Some reports exist that describe the donation of organic functional groups to calcium phosphate ceramics through covalent linkages with functional-group-terminated organic reagents. Nishizawa et al. reported that the surface hydroxyl groups of calcium phosphate ceramics formed covalent bonds with silane coupling [52]. Labella et al. speculated that the silane coupling agents could react with surface hydroxyl groups of HAp, and they developed a silanized HAp dental filler [53]. Dupraz et al. characterized the surface properties of silane-treated HAp powder with XPS and ζ-potential measurement [54]. Liu et al. first showed that the surface hydroxyl groups of HAp nanoparticles are reactive with isocyanate groups in organic reagents with solid ^{1}H Magic-Angle Spinning Nuclear Magnetic Resonance [55].

In this section, we demonstrated preparation methods of a novel composite consisting of a nanoscaled HAp particle and a polymer substrate—a silk fibroin (SF)

fiber—through covalent linkage and ionic interaction. Some methacrylate monomers—2-(o-[1′-methylpropylidenamino] carboxyamino) ethyl methacrylate (MOI-oxime) that is 2-methacryloxyethyl isocyanate (MOI) blocked by oxime, γ-methacryloxyethyl trimethoxysilane (MPTS), and 4-methacryloyloxyethyl trimellitate anhydride (4-META)—which have telechelic functional groups, such as alkoxysilyl, isocyanate, and anhydride groups have been used for reaction with HAp surface by chemical bonding as shown in Scheme 2.

The SF fiber shows good qualities for implant materials, such as good mechanical properties, moldability, possessing many functional groups on the surface, and actual results as a suture in the medical field for a long period. We selected SF as a polymer substrate to develop a composite with HAp since the SF fiber can add mechanical strength and flexibility to the inorganic material. The chemical modification of the HAp surface in advance is not necessary for the preparation of the composite.

3.2. HAp Coating by Covalent Bonding

3.2.1. Isocyanate Group

The composite was prepared through a two-step procedure—the graft-polymerization of poly(MOI-oxime) (Showa Denko Co., Tokyo, Japan) on the SF as the first step and coupling between HAp and the modified SF as the second step. This synthetic method is simpler and more reasonable compared with our previous three-step procedure [18], and MOI is a difunctional monomer with an isocyanate group and a vinyl double bond. The isocyanate group reacts easily with active hydrogen compounds, such as water. The blocked MOI derivative, for example, MOI-oxime, allows the benefit of MOI being extended into a water-based system [56].

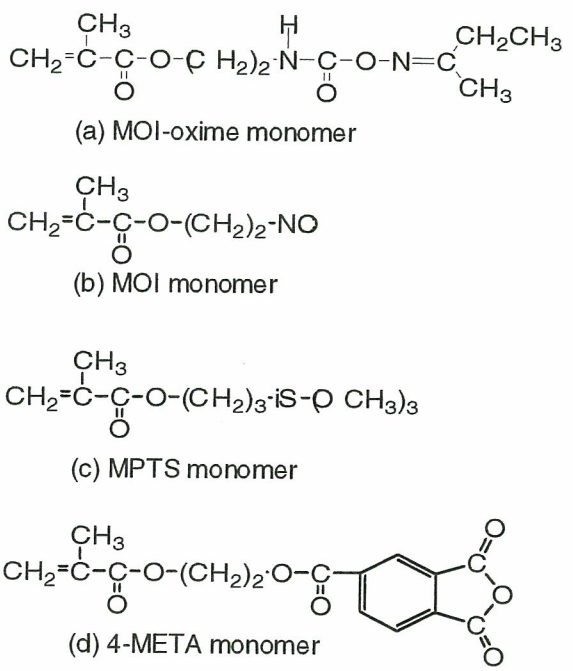

Scheme 2. Chemical structures of (a) 2-(o-[1′-methylproplidenamino] carboxyamino) ethyl methacrylate (MOI-oxime), (b) 2-methacryloxyethyl isocyanate (MOI), (c) γ-methacryloxyethyl trimethoxysilane (MPTS), and (d) 4-methacryloyloxyethyl trimellitate anhydride (4-META).

The MOI oxime was grafted on the SF using ammonium peroxodisulfate (APS) as an initiator, and pentaethylene glycol dodecyl ether as a nonionic surfactant. Graft-polymerization with MOI-oxime onto the SF was conducted by free radical initiation [57]. The SF fabric used in this reaction was degummed habutae fabric (Fujimura-Seishi Co., Kochi, Japan) made of silk from *Bomboyx mori* and was cleaned by a soxhlet extractor. The 339 ml (1.8 mmol) of the MOI-oxime monomer, 41 mg (0.18 mmol) of APS, and 73 mg (0.18 mmol) of the surfactant were mixed in 6.0 ml of distilled water. Five pieces of the SF (1.8 cm in diameter) were immersed in the reaction mixture in 50-ml thick-walled polymerization tubes. The tubes were degassed by freezing and evacuating three times and then sealed. Graft-polymerization was conducted at 45°C for different periods. Poly(MOI-oxime)-grafted fabrics were collected from the reaction system, washed with acetone followed by washing with distilled water to remove unreacted monomers and homopolymers, and finally dried by vacuum for 24 h at room temperature. The weight gain was calculated from the increase in weight of the dried original SF after graft-polymerization with MOI-oxime as follows:

$$\text{weight gain (wt\%)} = (W_2 - W_1)/W_1 \times 100,$$

where W_1 and W_2 are the dried weight of the original SF and poly(MOI-oxime)-grafted SF, respectively.

Figure 8 shows the ATR FT-IR spectra of the MOI-oxime monomer, the original SF, and the poly(MOI-oxime)-grafted SF. Peaks at 1621, 1514, and 1260/1230 cm^{-1} were attributed to amide I, II, and III, respectively, which are the typical absorbances of the SF substrate as shown in Figure 8(b). After the modification with the MOI-oxime,

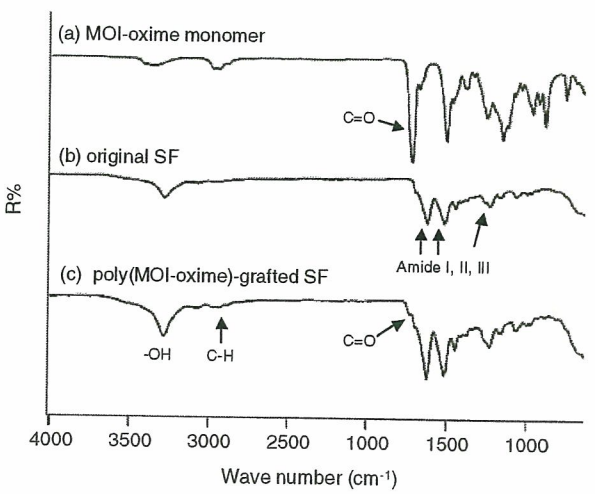

Figure 8. ATR FT-IR spectra of (a) MOI-oxime monomer, (b) original SF, and (c) (MOI-oxime)-modified SF.

new peaks appearing at 2936 and 1716 cm^{-1} contributed hydrocarbon and carbonyl groups of the monomer. It is clear that graft-polymerization of MOI-oxime is well conducted.

After HAp nanoscaled particles were suspended in toluene/isopropanol (9/1), a poly(MOI-oxime)-grafted SF was soaked in the suspended solution for 1 h at room temperature to be adsorbed on the SF. The SF adsorbed with the particles was washed by stirring in ethanol. This fabric with HAp was heated at 140°C for 20 min in vacuum at 1 mmHg for the deblocking of MOI-oxime and the reaction between the HAp particles and the isocyanate group of the grafted polymer. The composite was washed by using an ultrasonic generator for 3 min (output: 20 kHz, 35 W) to remove excess adsorbed HAp particles attached to ones in the same solution. Finally, the composite was washed in a great amount of distilled water for one day to remove the residual organic solvents used in the synthetic process.

The surface morphologies of HAp nanoparticles coated on a SF fiber explained in the next paragraph. To prove indirectly the formation of the urethane linkage between HAp particles and MOI-oxime, the reaction of the particles with the MOI-oxime monomer was carried out. Briefly, the HAp nanoparticles adsorbed with MOI-oxime were heated at 140°C for 20 min in vacuum at 1 mmHg and the product was washed by acetone to remove the unreacted reagents. Figure 9 shows the diffuse reflectance FT-IR spectra of the original and (MOI-oxime)-modified HAp nanoparticles. The spectrum of the (MOI-oxime)-modified HAp (Fig. 9(b)) shows additional absorption bands, with respect to the original particle spectrum, due to C-H stretch at 2978, C=O stretch of the ester group at 1724, C=O stretch of the urethane group at 1653, and N–H bending at 1575 cm^{-1}. This result is in accord with Liu's paper [58]. By heating in vacuum, the formation of the urethane linkage follows the release of oxime from MOI-oxime to generate the isocyanate groups [56], because the deblocking temperature of MOI-oxime is 140°C and the boiling point of oxime is 60°C. From the spectrum, it is estimated indirectly that HAp particles might be coupled with the isocyanate groups in poly (MOI-oxime)-grafted SF by the urethane linkage. It is possible to lower the reaction temperature by using MOI blocked with phenol or imidazole, for the deblocking temperature of these agents is 110–130°C [56]. This reaction system is, therefore, a unique method of fixing HAp on the polymer substrate.

3.2.2. Alkoxysilyl Group

Graft-polymerization with MPTS monomer having an alkoxysilyl group on SF fibers with 100 μm of length was conducted by free radical initiation. Initially, 1.8 mmol of the MPTS and 0.18 mol of a nonionic surfactant, pentaethylene glycol dodecyl ether, were thoroughly mixed and added to 50-ml thick-walled polymerization tubes. Subsequently, 0.18 mmol of APS in 6.0 ml of distilled water and 600 mg of SF fibers was added to the tubes. The tube was degassed by freezing, evacuated three times, and then sealed. Graft-polymerization was conducted at 50°C for different periods. Poly(MPTS)-grafted SF were collected from the reaction system, washed with 300 ml of dry-methanol and filtrated by a filter with a 5- μm cut-off point to remove unreacted monomers and homopolymers and dried by vacuum for 1 h at 60°C. After the HAp particles were suspended in a toluene/methanol (9/1) mixture solvent, a poly(MPTS)-grafted SF was soaked in the suspended solution for 1 h at room temperature to be adsorbed on the SF. The SF adsorbed with the HAp particles was washed by stirring in methanol and filtered by a filter with a 5- μm cut-off point to remove unreacted HAp particles. The fibers adsorbed with HAp were heated at 120°C for 2 h in vacuum at 1 mmHg for a reaction between the HAp surface and the alkoxysilyl groups of the graft polymers. The composite was washed by using an ultrasonic generator for 3 min (output: 20 kHz and 35 W) to remove excess adsorbed HAp particles attached to ones in ethanol. Finally, the composite was washed in a great amount of distilled water for one day to remove the residual organic solvents used in the synthetic process.

Graft-polymerization with MPTS possessing alkoxysilyl groups coupled with hydroxyl groups on the HAp surface on the SF substrate through a one-step procedure was conducted. Figure 10 shows the ATR FT-IR spectra of the poly(MPTS) homopolymer, unreacted SF and

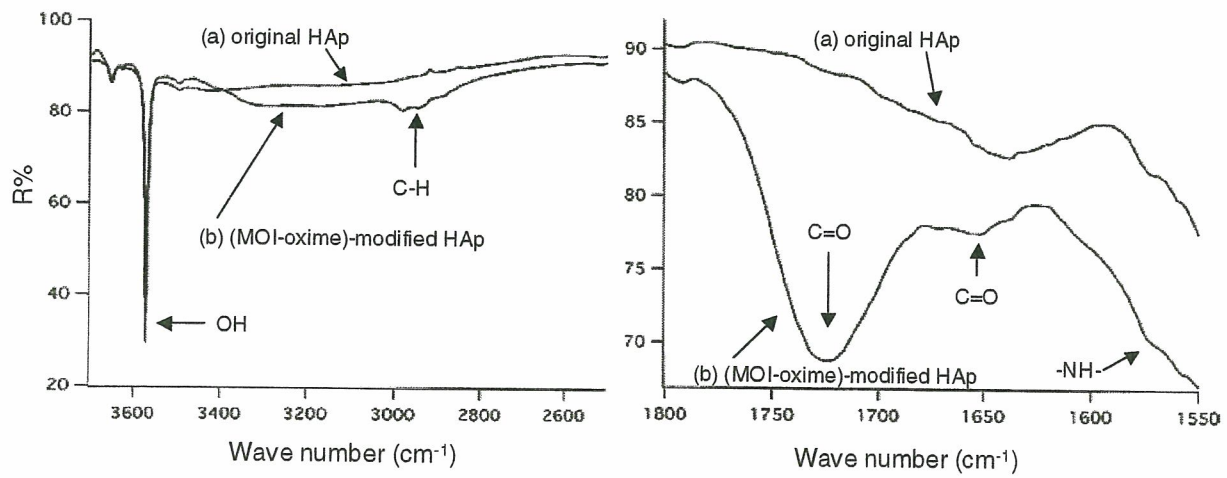

Figure 9. Diffuse reflectance FT-IR spectra of (a) original and (b) (MOI-oxime)-modified calcined HAp nanoparticles.

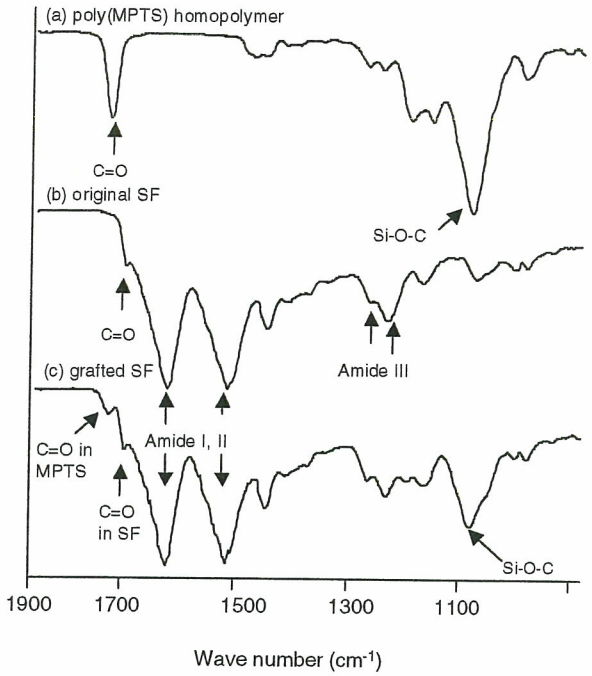

Figure 10. ATR FT-IR spectra of (a) poly(MPTS) homopolymer, (b) SF fiber, and (c) poly(MPTS)-grafted SF. Reprinted with permission from [21], T. Furuzono et al., *J. Artif. Organs* 7, 137 (2004). © 2004, Springer.

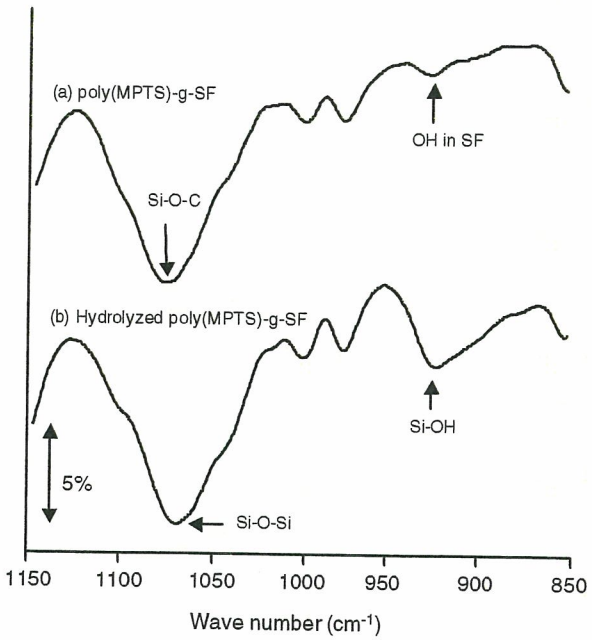

Figure 11. ATR FT-IR spectra of (a) poly(MPTS)-grafted SF just after preparation and (b) hydrolyzed poly(MPTS)-grafted SF. Reprinted with permission from [21], T. Furuzono et al., *J. Artif. Organs* 7, 137 (2004). © 2004, Springer.

the poly(MPTS)-grafted SF having 14.3 wt% of weight gain against intact SF. Typical peaks in the poly(MPTS) homopolymer can be seen at 1725 and 1076 cm^{-1} ascribed the C=O stretching vibration of ester groups and the Si-O-C stretching vibration of alkoxysilyl groups, respectively (Fig. 10(a)). The peaks at 1621, 1514, and 1260/1230 cm^{-1} were attributed to amide I, II, and III, respectively, which are the typical absorbances of the SF substrate, as shown in Figure 10(b). After graft-polymerization with poly(MPTS), a peak contributing to Si-O-C of the graft-polymer remains at 1076 cm^{-1} in Figure 10(c). Figure 11 shows ATR FT-IR spectra of the poly(MPTS)-grafted SF just after preparation and the sample treated by hydrolysis with water in an autoclave. In the spectrum of the poly(MPTS)-grafted sample (a), the Si-O-C stretching vibration attributed to the graft-polymer at 1076 cm^{-1} and the OH stretching vibration belonging to the SF substrate at 926 cm^{-1} were recognized. However, two new peaks appear at 1068/922 cm^{-1} belonging to the Si-O-Si and Si-OH stretching vibrations, respectively, in the spectrum of the hydrolyzed sample (b). This means that the alkoxysilyl groups of the graft-polymers just after preparation avoided hydrolysis, and maintained their activity in coupling with the hydroxyl groups on the HAp surface regardless of using water as the reaction solvent. The surfactant in the reaction solvent was effective in protecting the active groups from hydrolysis. In our previous study, graft-polymerization having alkoxysilyl groups was achieved through a vinyl bond of 2-methacryloxyethyl isocyanate (MOI) bonded on the SF substrate in anhydrous organic solvents via a two-step procedure [19]. It can be mentioned that the alternative graft-polymerization system in this section is technically easier and more advantageous compared to the former method due to using water as the solvent and the single-reaction procedure.

Figure 12 shows the ATR FT-IR spectrum of the calcined HAp nanoparticles coated on poly(MPTS)-grafted SF. The weight gain of HAp particles coated on SF was 13.2 wt% determined by a thermogravimetric analysis (TGA). The peak at 3572 cm^{-1} belongs to the OH stretching vibration of highly crystalline HAp coated on SF. This peak is very small because a signal intensity of the ATR FT-IR spectrum shows the specific character that is weaker in a higher wave-number region than that in a lower region. The peaks at 1091 and 1052 cm^{-1} reflect $\nu_3(PO_4^{3-})$ of the HAp crystals. The peak at 3281 cm^{-1} shows OH stretching of amino acids in SF because there are many hydroxyl residues such as 10.63 mol% of Ser, 4.97 mol% of Tyr, and 0.89 mol% of Thr in SF. Although the bands attributed to the Si-O-Si stretching vibration at 1068 cm^{-1} or Si-OH at 922 cm^{-1} generated by hydrolysis of poly(MPTS) cannot be seen due to an overlap of the peaks attributed to the PO_4^{3-} stretching vibration of HAp at around 1100–900 cm^{-1}, the peaks of amide I/II and two C=O from poly(MPTS) and the SF substrate at 1621/1514 and 1725/1696 cm^{-1}, respectively, can be clearly observed. This means the coating of HAp particles did not fully and thickly cover the surface of grafted SF. The existence of covalent bonds between the HAp particles and the poly(MPTS)-grafted SF was estimated by an indirect method using an FT-IR measurement [18].

As the evidence of existence of covalent linkage, in the FT-IR spectrum of the heating product of the mixture with the HAp nanoparticles and the MPTS monomer at 120°C

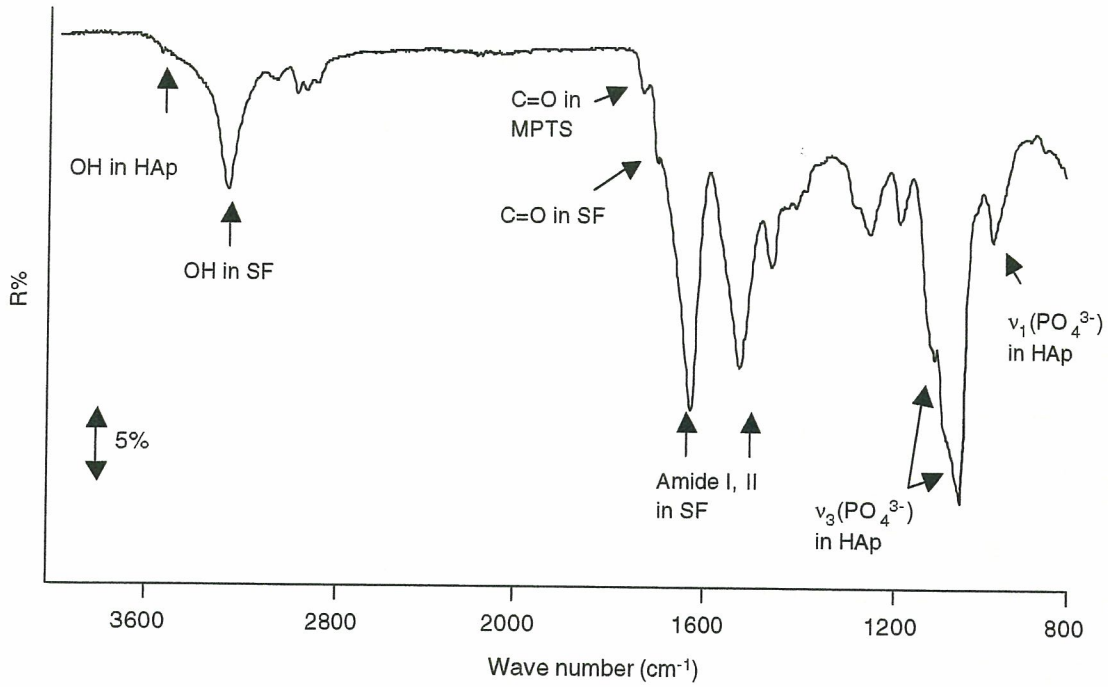

Figure 12. ATR FT-IR spectrum of calcined HAp particles covalently coated on SF fibers. Reprinted with permission from [21], T. Furuzono et al., *J. Artif. Organs* 7, 137 (2004). © 2004, Springer.

for 2 h in vacuum, a new peak appeared at 1043 cm^{-1} [18]. This band is known as the sign belonging to an Si-O stretching vibration from the covalent bond between the HAp and silane coupling agent [52].

Figure 13 shows an SEM photograph of the HAp-coated SF fiber with 13.1 ± 1.2 wt% ($n = 4$) in the composite determined by TGA. The weight gain of HAp particles on the SF fiber increased about 5 times compared to that on the SF fabric, 2.8 ± 0.5 wt% by the same preparation conditions. This means that it is hard for nano-HAp particles to penetrate into and coat on gaps between fibers in the SF fabric.

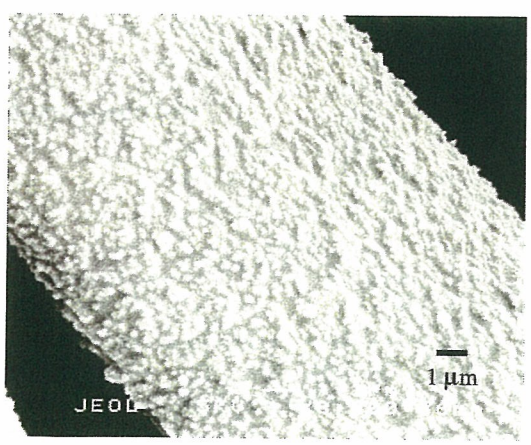

Figure 13. SEM photograph of calcined HAp nanoparticles covalently coated on an SF fiber. Reprinted with permission from [21], T. Furuzono et al., *J. Artif. Organs* 7, 137 (2004). © 2004, Springer.

In other words, a fiber cut approximately 100 μm in length was more effective for the coating than that of a fabric form. The HAp particles separated or aggregated into several crystals under SEM observation. Aggregation was easy because the HAp monoparticle has an *a*-plane with a cationic charge and a *c*-plane with an anionic charge in a monocrystal [59]. It was difficult, therefore, to prepare perfect monolayer with HAp nanoparticles separately on the SF surface.

3.3. HAp Coating by Ionic Bonding

3.3.1. Carboxyl Group

In the former subsections, the coupling method between HAp nanoparticles and a polymer substrate through covalent linkage was mentioned. This synthetic way needs, however, one more step, which is thermal treatment above 100°C in a vacuum to connect HAp to SF by covalent linkage, besides the physical adsorption of HAp on the SF. This system is not useful when applying it to the non-heat-resistant biomedical material such as polyethylene and is industrially disadvantageous. In this subsection, to couple HAp particles and SF under a nonheat condition, therefore, we applied graft-polymerization with 4-methacryloyloxyethyl trimellitate anhydride (4-META) onto the SF by free radical initiation. The 4-META has already been applied to resin monomers for dental surgery and is harmless to a living body. Moreover, the methyl methacrylate (MMA) resin with 4-META had larger tensile bond strength compared with the MMA resin without 4-META because of the strong affinity between HAp and 4-META [60]. Here, we report on the synthesis and bioactivity of the novel HAp/SF composite using 4-META.

Graft-polymerization with 4-META onto the SF was conducted by free radical initiation [57], with 273.80 mg (0.9 mmol) of the 4-META monomer, 41 mg (0.18 mmol) of APS, and 73 mg (0.18 mmol) of the surfactant were mixed in 6.0 ml of distilled water. The 74.94 mg of the SF fabric (18 mm in diameter) was immersed in the reaction mixture in 50-ml thick-walled polymerization tubes. The tubes were degassed by freezing and evacuating three times and then sealed. Graft-polymerization was conducted at 50°C for different periods. The poly(4-META)-grafted fabrics were collected from the reaction system, washed with acetone followed by washing with distilled water to remove unreacted monomers and homopolymers, and finally dried by vacuum for 24 h at room temperature.

The poly(4-META)-grafted SF was immersed in a 0.01 M potassium hydroxide aqueous solution for 10 min and the five-member ring of this SF was opened and ionized. After HAp nanoscaled particles were suspended in toluene/methanol (8.8/1), an ionized poly(4-META)-grafted SF was soaked in the suspended solution for 1 h at room temperature to be adsorbed on the SF. The SF adsorbed with the particles was washed by stirring in acetone to remove the solvent. The composite was washed in distilled water by using an ultrasonic generator for 3 min (output: 20 kHz, 35 W) to remove excess adsorbed HAp particles. Finally, the composite was freeze-dried by vacuum for one day to evaporate the residual water.

Figure 14 shows the ATR-FTIR spectra of the 4-META monomer, the original SF, the poly(4-META)-grafted SF, and the ionized poly(4-META)-grafted SF. The peaks at 1621, 1514, and 1260/1230 cm^{-1} were attributed to amide I, II, and III, respectively, which are the typical absorbances of the SF substrate as shown in Figure 14(b). After modification with the 4-META monomer (Fig. 14(c)), new peaks contributing to the monomer appeared due to the C=O stretching vibration of –CO–O–CO– at 1724 cm^{-1} and ester groups at 1696 cm^{-1}, and the C-O stretching vibration of ester groups at 1158 cm^{-1}. After ionization of the grafted SF (Fig. 14(d)), the peak of the C=O stretching vibration of –CO–O–CO– disappeared and new peaks at 1392 and 1367 cm^{-1} attributed to the symmetric vibration of –COO– appeared.

To estimate indirectly the formation of ionic interaction, HAp particles connected with ionized 4-META were prepared. The HAp particles were adsorbed with 4-META, ionized by a 0.1 M potassium hydroxide aqueous solution in toluene/methanol (8.8/1) for 1 h. The reactant was washed with distilled water to remove the unreacted reagents and dried by heating at 120°C under vacuum.

In Figure 15, the solid line shows the difference FT-IR spectrum which subtracts the original HAp from the HAp particles with ionized 4-META. The peak of 1368 cm^{-1} demonstrates the existence of $-COO^-$. This absorption band shifted by 6 cm^{-1} to a lower side of wave number in comparison with ionized 4-META (dotted line, 1374 cm^{-1}). This shift suggests that carboxylate groups in ionized 4-META interacted with Ca^{2+} ions on the surface of HAp [61, 62]. From these spectra, it is estimated indirectly that HAp nonoparticles might be coupled with $-COO^-$ groups in the ionized poly(4-META)-modified SF by the ionic interaction.

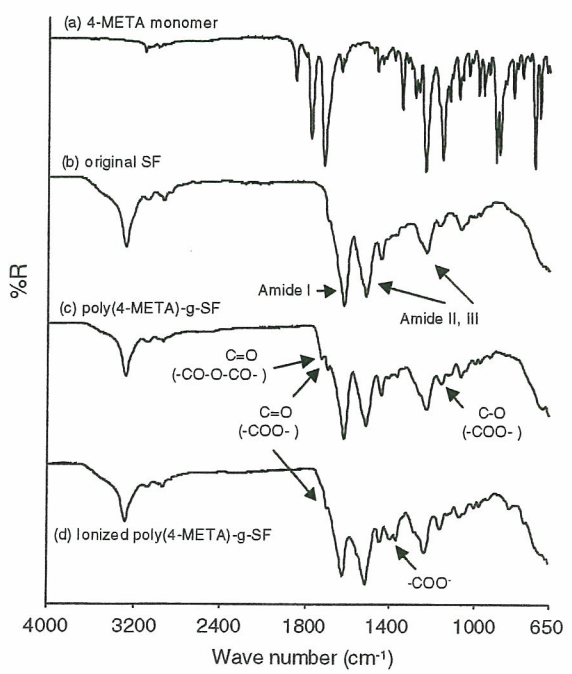

Figure 14. ATR FT-IR spectra of (a) 4-META monomer, (b) original SF, (c) poly(4-META)-grafted SF, and (d) ionized poly(4-META)-grafted SF.

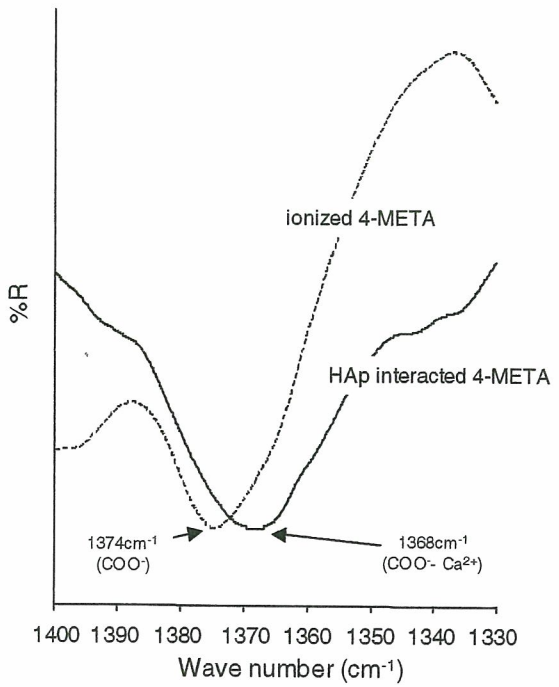

Figure 15. Difference FT-IR spectrum of diffuse reflectance which subtracts original HAp from HAp nanoparticles with ionized 4-META (solid line) and FT-IR spectrum of the ionized 4-META monomer (dashed line) at 1400–1330 cm^{-1}.

This synthetic procedure of the composite is outlined in Scheme 3.

By using the mixture of toluene and methanol, the HAp nanoparticles are equally dispersed in the medium and are adsorbed physically and dispersively on the SF surface because of the strong affinity between HAp and 4-META [8]. The SF, after ring-opening using a potassium hydroxide aqueous solution, moreover, has carboxylate groups on the surface. It is well known that the *a*-plane of HAp has a cationic surface which consists of Ca^{2+} ions [59]. It seems, therefore, that the *a*-plane of HAp was adsorbed on the SF covered with carboxylate groups. When the SF adsorbed with particles is washed in distilled water, K^+ ions are released from the SF, and $-COO^-$ in the ionized SF is coupled with the Ca^{2+} ions of HAp particles by ionic interaction due to the ionization tendency. In the series of our articles on the HAp/SF composite [18, 19, 21], the hydroxyl groups of HAp were needed to couple between the HAp nanoparticles and the SF substrate. In this synthetic method, however, these groups are not necessarily required, because the HAp particles are connected with the SF substrate by ionic interaction. By using 4-META, it is expected that not only HAp but also other inorganic compounds, such as β-tricalcium phosphate (β-TCP), can be adsorbed and connected on the SF fiber surface. In this way, HAp nonoparticles can be connected with modified SF under a nonheat condition, compared with the conventional way. This condition is useful when using non-heat-resistant biomedical material, such as polyethylene, as a polymer substrate for synthesizing the HAp/polymer composite.

3.4. Mechanical Properties

The tensile properties were measured by using TENSILON RTC-115 OA (ORIENTEC Co., Tokyo, Japan) at an elongation rate of 5 mm/min and 25°C. To determine the mechanical properties of the composite, a suture-like composite made of Kinsyu x Syowa (a variety of silk) was adopted. The unit of stress value was changed from *g/d* to *Pa* as shown by the following equations [63].

$A_0 = d/(9 \times 10^5 r)$,

A_0: cross-section area (cm^2),

d: denier (the experimental value = 97),

r: specific gravity (1.33 g/cm^3)

$S = P/(A_0 \times 10{-}^4)$

S: stress (Pa), P: experimental value of stress (N).

Data from the tensile test are presented as plus or minus standard deviation for the mean. Statistical comparisons were performed with the use of the Student's *t*-test and p values <0.01 were considered.

Figure 16 shows the tensile properties of three types of SF fiber (original SF, graftpolymer-grafted SF, and HAp/SF

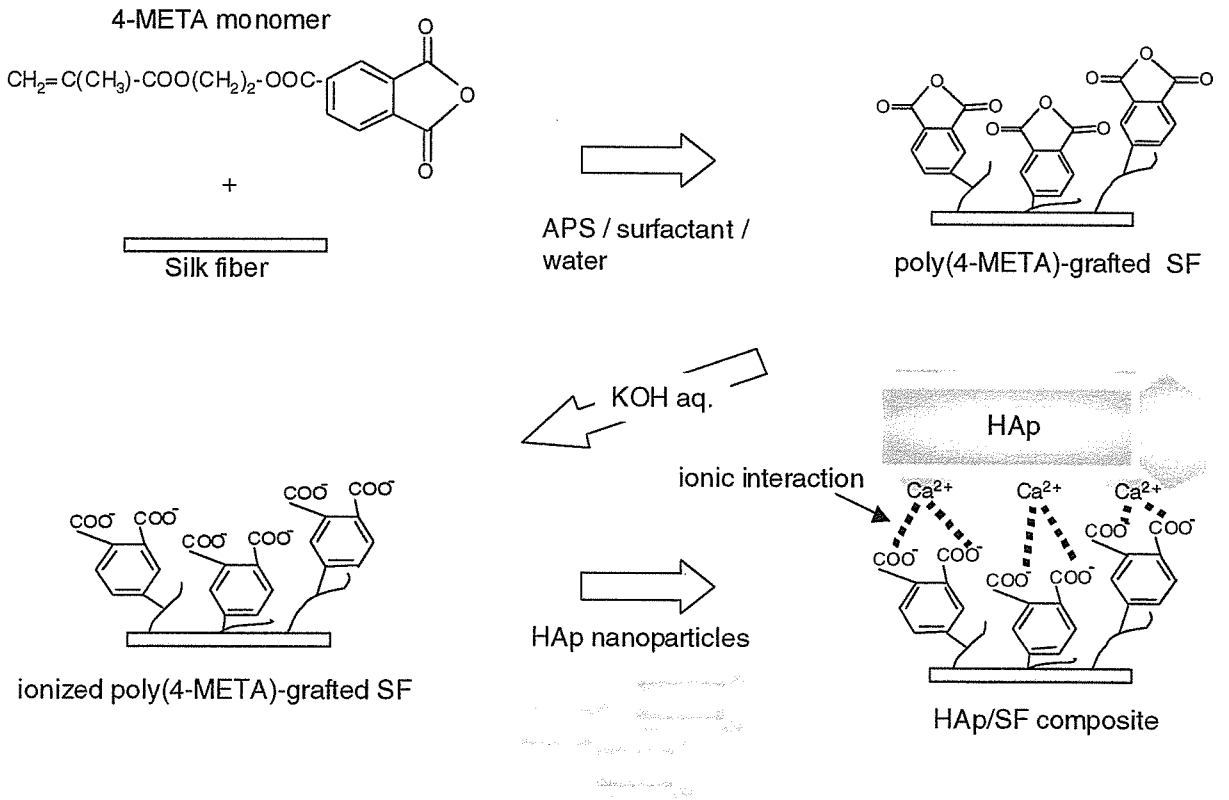

Scheme 3. Schematic presentation of the synthesis of the HAp/SF composite by ionic bonding.

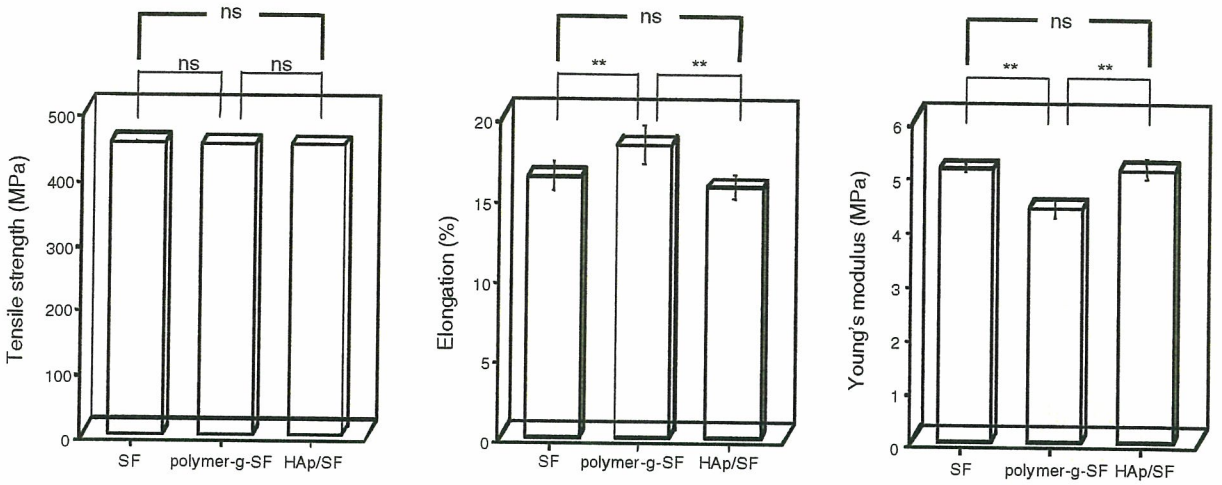

Figure 16. Mechanical properties of three types of SF fibers [original SF, (MOI-oxime)-grafted SF, and HAp/SF composite fiber]. Data were calculated as means of six-time determinations. Error bars represent standard deviations of six-time determinations. **means an existence of a significant difference ($P < 0.01$) between two samples.

composite). The tensile strengths, the elongation at break, and Young's modulus between the original SF and the HAp/SF composite were unchanged. Compared with the original SF and HAp/SF composite, the elongation at break of graftpolymer-grafted SF was somewhat higher but Young's modulus and thereof was somewhat lower, statistically. These results suggest that the difference of the elasticity may depend on the crystallinity on the surface. By means of the graft-polymerization on the SF, the crystallinity on the surface of SF decreases. The elasticity of polymer-grafted SF, therefore, decreases. After the coupling between HAp and the modified SF, it seems that the crystallinity is compensated by the covering with the inorganic substrate on the surface of SF and the elasticity of the HAp/SF composite is apparently equal to that of the original SF. These results show that this HAp/SF composite maintains flexibility equivalent to the original SF.

3.5. Cell Interaction

Mouse fibroblast cell lines of L929 cells were cultured in a complete α-minimum essential medium (α-MEM, Invitrogen Corporation, Tokyo, Japan), supplemented with heat-inactivated 10% fetal bovine serum (FBS, Gibco), 50 IU/ml of penicillin, 50 μg/ml of streptomycin, and 2.5 μg/ml of amphotericin B (ICN Biomedicals, Inc., Calif.). To detect cell adhesiveness on the samples, cell morphologies were observed by SEM. The L929 cells (1×10^5 cells/ml) were plated onto 24-well multiplates with fabric samples of 1.5 cm in diameter in an α-MEM with 10% FCS and incubated at 37°C for 24 h. As for the button-shaped samples, however, after the samples were immersed into 1.5-ml microtubes with 1.0 ml of the culture medium, an ultrasonic treatment was conducted via the tubes to remove gases from the gaps of the fibers for 1 min. The L929 cells were subsequently plated in the microtubes with the samples at 1×10^6 cells/tube in an α-MEM with 10% FCS and incubated at 37°C for 48 h. After being washed with phosphate-buffered saline [PBS(−)] three times, the samples were fixed with 2.5% buffered-glutaraldehyde for 20 min at 30°C. The cells were dehydrated with aqueous ethanol (30–100%) and 100% *n*-butanol for 5 min at room temperature step by step. The samples were lyophilized and coated with gold.

To evaluate the cell adhesiveness on the HAp-coated SF, the morphologies of L929 fibroblast cells incubated on sample fabrics or devices were observed by SEM. Figure 17 shows SEM observations of the surfaces of sample fabrics—gelatin-coated glass as a positive control (a), untreated SF (b), hydrolyzed poly(MPTS)-grafted SF (c) and HAp-coated SF (d)—incubated with L929 cells for 24 h. The cells hardly adhered on the hydrolyzed poly(MPTS)-grafted

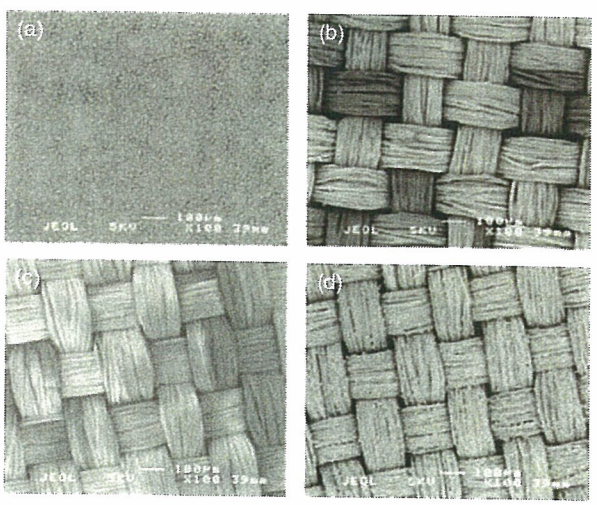

Figure 17. SEM photographs of cell morphologies on (a) gelatin-coated grass, (b) original SF fabric, (c) hydrolyzed poly(MPTS)-grafted SF fabric, and (d) calcined HAp nanoparticles covalently coated on an SF fabric. Reprinted with permission from [21], T. Furuzono et al., *J. Artif. Organs* 7, 137 (2004). © 2004, Springer.

SF as well as the untreated SF in Figure 17(b) and 17(c). Although it has been known that the initial cell adhesion on intact SF is actually not good [19, 20], the reason has not been thoroughly manifested. It is presumed to depend on high surface wettability due to containing many hydrophilic amino acid residues[17]—the hydroxyl group: Ser 10.63 mol%, Tyr 4.97 mol%, Thr 0.89 mol%; the carboxyl group: Asp 1.65 mol%, Glu 1.21 mol%; the amino groups: Lys 0.33 mol%, His 0.18 mol%, Arg 0.49 mol%—and peptide bonds without an arrangement of Arg-Gly-Asp (RGD) as a cell-adhesion molecule, or probably the existence of a microdomain structure [64] consisting of crystalline and amorphous regions attributed to an arrangement of $(Gly\text{-}Ala\text{-}Ser)_n$ and the other residues in SF. The cells indicated weak interaction with the hydrolyzed poly(MPTS)-grafted surface during the initial incubation period because of the surface hydrophilicity belonging to Si-OH moieties on Si-O-Si cross-linking networks produced by hydrolysis of the poly(MPTS)-grafted SF substrate demonstrated by ATR FT-IR analysis in Figure 11. Meanwhile, the cells adhered well on HAp-coated SF similarly to the previous reports [19, 20, 26] and as shown in Figure 17(d). The cross-sectional view of the composite with a cell stained shown in Figure 18. The needle-like microspikes from a cell incubated for 24 h were elongated to a calcined HAp nanoparticle chemical bonded on the polymer substrate. Cells, thus, favorably adhere only on the HAp surface of the composite but not on the dehydrated grafted-surface without HAp particles on the SF substrate. It is estimated that cell-adhesion proteins in serum, such as fibronectin, vitronectin, bFGF, and so, before cell adhesion, adsorb on a HAp surface much better than on an area of dehydrated graft-polymer (Scheme 4).

We previously reported that L929 cells restrictedly elongate their needle-like microspikes against an amino group-modified TiO_2 (TiO_2-NH_2) surface but that poly(acrylic acid(AAc))-grafted regions on the composite of TiO_2-NH_2 nanoparticles covalently linked onto a polyAAc-grafted silicone substrate [65]. A similar phenomenon takes place in the interface between a cell and a HAp composite on a nanoscaled HAp-coated SF substrate. That is to say, sintered HAp nanoparticles can provide bioactivity to a polymer substrate.

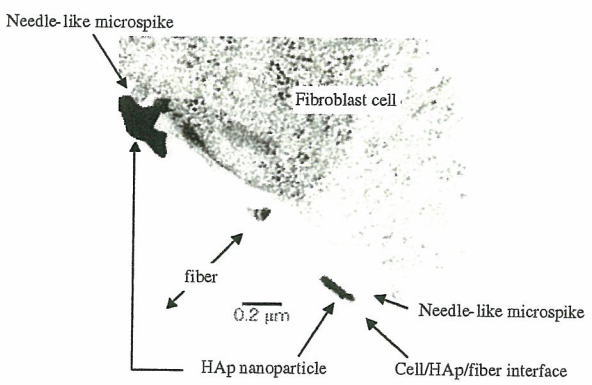

Figure 18. TEM micrograph of cross-sectional view of fiber/HAp/cell interface. The stained sample which is fibroblast incubated on HAp/SF for 24 h was cut by microtome. Reprinted with permission from [21], T. Furuzono et al., *J. Artif. Organs* 7, 137 (2004). © 2004, Springer.

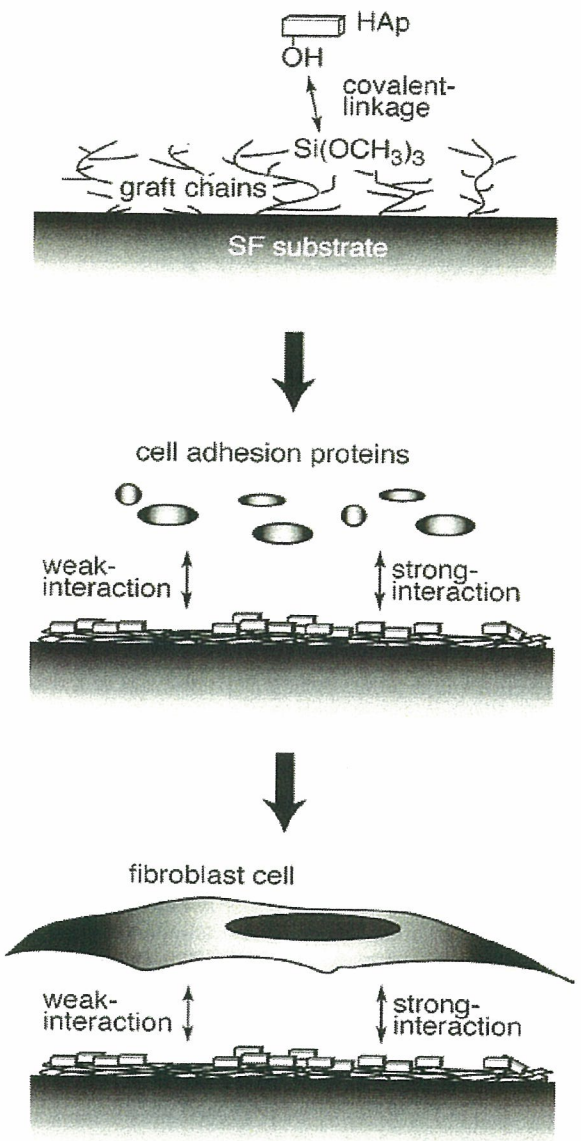

Scheme 4. Schematic presentations of the preparation of the composite and the expected mechanism of cell adhesion on calcined HAp nanoparticles coated SF. Reprinted with permission from [21], T. Furuzono et al., *J. Artif. Organs* 7, 137 (2004). © 2004, Springer.

4. FABRICATION OF MEDICAL DEVICES

4.1. A Percutaneous Device

A polymer substrate for a button form was molded using a silicone compound (KE153-U, Shin-Etsu Chemical Co. Ltd., Tokyo, Japan) to fix the pattern (Fig. 19). The internal diameter was based on the external diameter of a catheter for intravenous hyperalimentation (IVH). Silicone buttons covered with a silicone adhesive (TSE399, GE Toshiba Silicones Co., Ltd., Tokyo, Japan), which were then attached to a rotator on a motor that revolved at 450 rpm, by which HAp/SF fibers of about 100 mm in length thoroughly coated

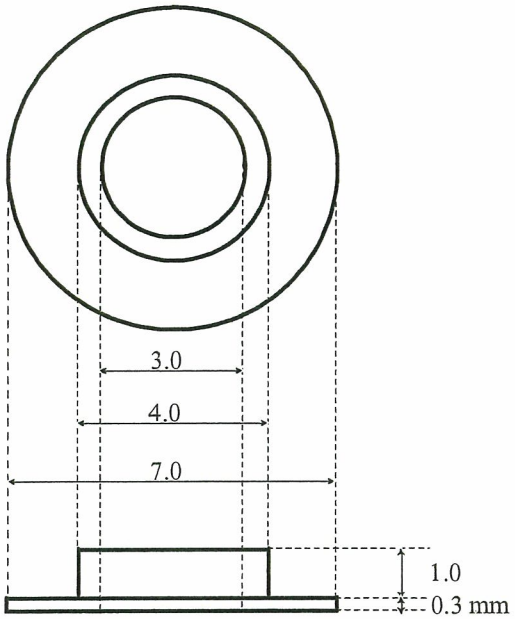

Figure 19. Design of a prototype model of a percutaneous button. Reprinted with permission from [21], T. Furuzono et al., *J. Artif. Organs* 7, 137 (2004). © 2004, Springer.

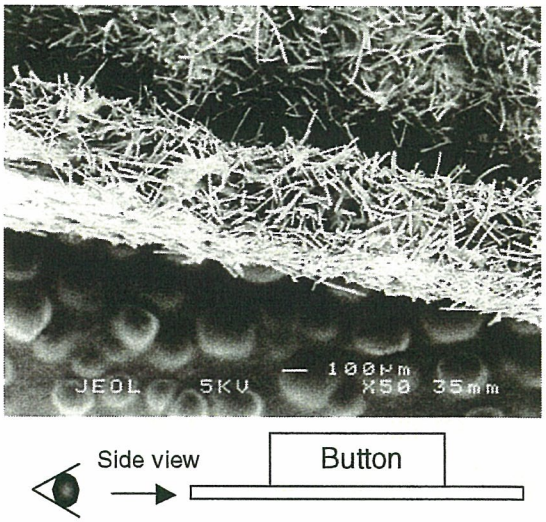

Figure 21. Magnified view of the edge of the button by SEM observation. Reprinted with permission from [21], T. Furuzono et al., *J. Artif. Organs* 7, 137 (2004). © 2004, Springer.

the buttons. The HAp/SF fiber-coated samples were heated at 120°C for 2 h in vacuum and were then washed in distilled water by using an ultrasonic generator for 3 min (output: 20 kHz, 35 W) to remove the fibers which adhered incompletely.

To fabricate a prototype for a percutaneous device, the HAp-coated SF fibers were transplanted onto a button-shaped substrate made of silicone via an adhesive agent. The weight ratio of three-dimensional coating consisting of composite fibers versus the total weight of the device was 14.3 ± 0.4 wt% ($n = 4$). The prototype of a button was fabricated by a silicone compound cast into a mold according to the illustration shown in Figure 19. The form was designed to install it a catheter for IVH whose outer diameter of tube showed 3.0 mm. Figure 20 shows the external appearances of the button allowing the catheter tube through. The device is white and very flexible. Figure 21 shows a magnified view of the edge of the button coated with HAp-modified SF fibers. The HAp-coated SF fibers of 100 μm in length were uniformly transplanted individually in random directions on the button.

A cell adhesion experiment using fibroblast cells was also conducted via the sample device. After incubation of untreated SF or HAp-coated SF buttons in a microtube for 48 h, the morphologies of the cells on both substrates were observed by SEM (Fig. 22). On HAp-coated SF buttons, the cells adhered and spread widely on the side surface. More spherical cells accumulated on other cells spread on the upper side of the button than on the side. This phenomenon shows that adhering cells accumulated in a multiple way on the substrate according to gravity in a three-dimensional incubation. However, few spherical cells were observed on untreated SF fibers transplanted on the button. These phenomena were equally consistent with the tendency of cell adhesiveness on the fabric samples. The three-dimensional composite is, therefore, useful as a cell

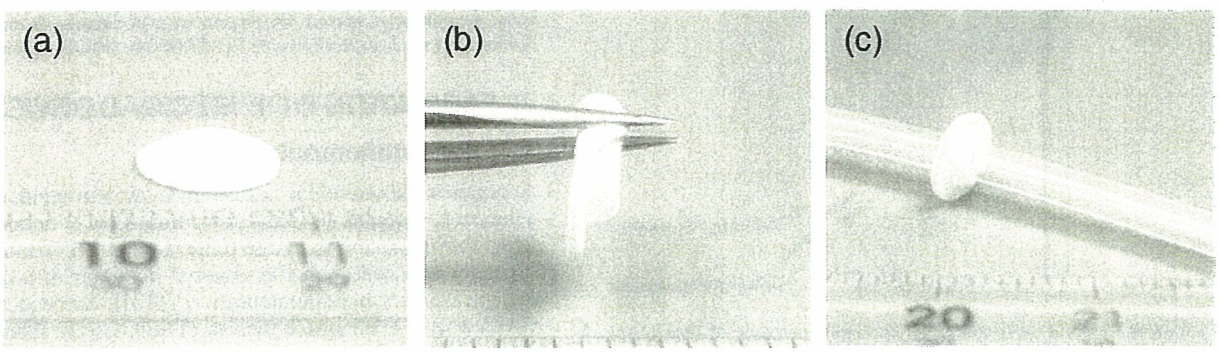

Figure 20. External views of the button prototype of a percutaneous device; (a) side view of the button, (b) flexibility of the button, and (c) a silicone tube installed in the button. Reprinted with permission from [21], T. Furuzono et al., *J. Artif. Organs* 7, 137 (2004). © 2004, Springer.

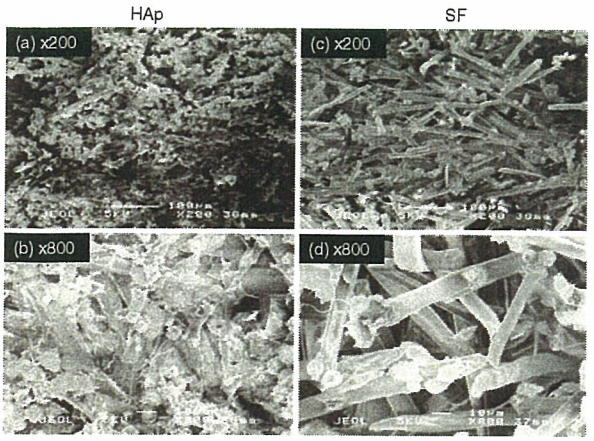

Figure 22. SEM photographs of cell morphologies on the upper views of the button made of (a, b) HAp-coated SF fibers and (c, d) untreated SF fibers. The magnification for (a, c) is ×200 and for (b, d), ×800. Reprinted with permission from [21], T. Furuzono et al., *J. Artif. Organs* 7, 137 (2004). © 2004, Springer.

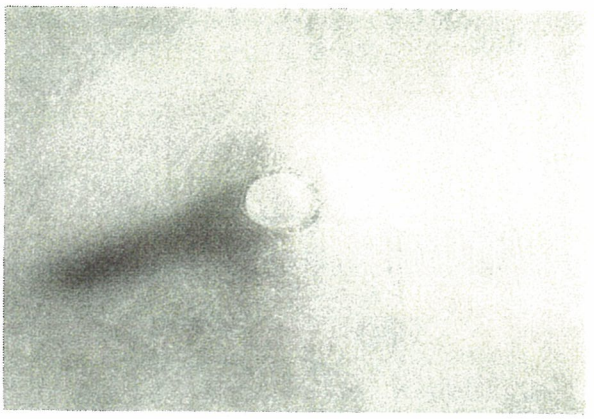

Figure 23. External view of the HAp-coated device percutaneously implanted into back of a rabbit for three months. The protruding substance is silicone tube, and HAp-coated percutaneous button is implanted just under the epidermis.

scaffold. The percutaneous device was implanted in back of a rabbit for three months, according to the Guideline for Animal Experimentation National Cardiovascular Center. The skin tissue was adhered on the device without a gap between the tissue and the material surface, and severe inflammation and abscess was not observed from the external view (Fig. 23).

4.2. An Artificial Blood Vessel

We developed a novel inorganic-organic composite, consisting of calcined HAp nanoparticles chemically bonded on polymer substrate. HAp nanoparticles were covalently linked onto a poly(ethylene terephthalate) (PET) fabric substrate chemically modified by graft polymerization with MPTS for development of artificial blood vessel. Figure 24 shows SEM images of human umbilical vein endothelial cells (HUVEC) morphologies and fluorescence images of stained nuclei of HUVEC on sample substrates after 4 h of incubation. The initial interaction of HUVEC on substrates was evaluated after 4 h of incubation, according to several reports [66, 67]. In the SEM images, it seemed that many cells adhered on HAp/PET fabric as well as collagen-coated PET, while only a few cells adhered on the original fabric. The difference in the number of cells that adhered could not be distinguished by SEM observation, since HUVEC were flattened and spread over the substrate. The cells adhered were then stained by fluorescent dye and

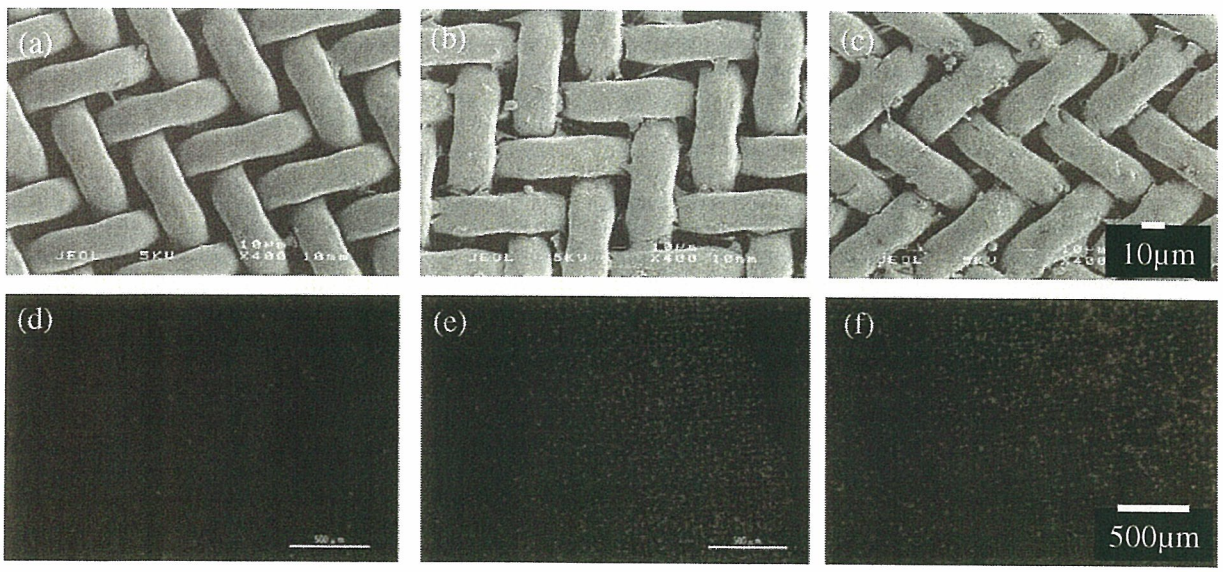

Figure 24. SEM and fluorescence photographs of HUVEC adhering on (a, d) original PET (b, d), collagen-coated PET, and (c, f) HAp/PET composite.